ThC4 (Invited)
9:30 am – 10:00 am

HIGH-RESOLUTION PHOTOACOUSTIC TOMOGRAPHY

Lihong V. Wang*, Xueding Wang, Geng Ku, Xueyi Xie, George Stoica

Optical Imaging Laboratory, Department of Biomedical Engineering
Texas A&M University, 3120 TAMU, College Station, Texas 77843-3120
URL: http://oilab.tamu.edu; Email: LWang@tamu.edu
** Corresponding author.*

Abstract: Optical contrast is sensitive to physiological parameters, such as the oxygen saturation and total concentration of hemoglobin, in biological tissues. Photoacoustic tomography is based on the high optical contrast yet utilizing the high ultrasonic resolution. Our work in this emerging area of research will be summarized in this invited talk. In this technology, a diffraction-based inverse-source problem is solved in the image reconstruction, for which we developed the rigorous reconstruction theory. We implemented a prototype and accomplished non-invasive transdermal and transcranial functional imaging of small-animal brains *in vivo*. Changes in the cerebral blood oxygenation and blood volume of a rat, as a result of the alternation from hyperoxia to hypoxia, were imaged successfully.

Keywords **– Photoacoustic tomography; optical contrast; ultrasonic resolution; inverse-source reconstruction; oxygen saturation of hemoglobin**

I. INTRODUCTION

Photoacoustic tomography (PAT, also referred to as optoacoustic or thermoacoustic tomography) involves both photons and ultrasound. A short-pulsed laser source is used to irradiate the biological tissue samples under investigation. A temperature rise of the order of mK will be produced in a short time frame. Consequently, thermoelastic expansion will cause emission of acoustic waves, referred to as photoacoustic waves. The photoacoustic waves are measured by wideband ultrasonic transducers around the sample, and the acquired photoacoustic waves are used to reconstruct the optical absorption distributions. Because the laser pulse is short, proportionately high frequency ultrasonic waves will be produced, which can provide diffraction-limited spatial resolution. In summary, the contrast in PAT is determined primarily by the optical properties of the biological tissues, and the spatial resolution in PAT is determined primarily by the photoacoustic waves originating from within the biological tissues.

II. FUNDAMENTALS OF PHOTOACOUSTICS: RECONSTRUCTION ALGORITHM

If the electromagnetic pumping pulse duration is much shorter than the thermal diffusion time through a voxel, thermal diffusion can be neglected; this is known as the thermal confinement. In this case, the acoustic wave $p(\mathbf{r},\bar{t})$ is related to electromagnetic absorption, $H(\mathbf{r},\bar{t})$, by the following wave equation:

$$\frac{\partial^2 p(\mathbf{r},\bar{t})}{\partial \bar{t}^2} - \nabla^2 p(\mathbf{r},\bar{t}) = \frac{\beta v_s}{C}\frac{\partial H(\mathbf{r},\bar{t})}{\partial \bar{t}}, \qquad (1)$$

where $\bar{t} = tv_s$; v_s is the acoustic speed, assumed to be constant; C is the specific heat; and β is the coefficient of volume thermal expansion. $H(\mathbf{r},\bar{t})$ can further be written as the product of a purely spatial component $\varphi(\mathbf{r})$ that describes the electromagnetic absorption properties of the medium at $\mathbf{r}$ and a purely temporal component $\eta(\bar{t})$ that describes the shape of the irradiating pulse.

Our group derived the exact inverse solutions in planar, spherical, and cylindrical geometries [1–3]. When the distance between the photoacoustic sources and the detector is much longer than the wavelengths of the high-frequency photoacoustic waves that are useful for imaging, the following approximate inverse solution holds:

$$\varphi(\mathbf{r}) = C\iint_{S_0} dS_0 \cos(\theta_d)\frac{1}{t}\frac{\partial p(\mathbf{r}_0,t)}{\partial t}\bigg|_{t=|\mathbf{r}_0-\mathbf{r}|/v_s}, \qquad (2)$$

where C is a constant; S_0 is the surface of detection; and θ_d is the angle between the normal of dS_0 and $\mathbf{r}-\mathbf{r}_0$.

III. EXPERIMENTS

The experimental system for PAT of a rat brain *in vivo* has been described before [see Ref. (4)]. In this work, through the modulation of the inhaled oxygen concentration, we changed the systemic physiological status of the rat. Firstly, provided with pure oxygen, the rat was under the hyperoxia status. Two photoacoustic images of optical absorption in the cerebral cortex of the rat brain were acquired with laser light at the 584-nm and the 600-nm wavelengths, respectively [see Figs. 1(A) and (B)]. Then the breathing gas was changed slowly to a mixed gas with a low concentration of oxygen (~8% O_2, ~5% CO_2 and ~87% N_2). Then, under the hypoxia status, another two images of the cerebral cortex corresponding to the same two wavelengths were acquired (not shown). With the high optical contrast between the blood and background brain tissues, each brain image presents the vascular structure in the cerebral cortex clearly and matches well with the open-skull anatomical photograph obtained after the photoacoustic imaging experiment [see

Fig. 1(G)].

For each physiological status, the two images of the relative optical absorptions at the two wavelengths enable us to compute the point-by-point hemoglobin oxygen saturation (SO_2) and total concentration of hemoglobin (HbT) in the cortical venous vessels through the following equations:

$$SO_2 = \frac{[HbO_2]}{[HbO_2]+[Hb]} = \frac{\mu_a^{\lambda_2}\varepsilon_{Hb}^{\lambda_1} - \mu_a^{\lambda_1}\varepsilon_{Hb}^{\lambda_2}}{\mu_a^{\lambda_1}\varepsilon_{\Delta Hb}^{\lambda_2} - \mu_a^{\lambda_2}\varepsilon_{\Delta Hb}^{\lambda_1}}, \quad (3)$$

$$HbT = [HbO_2]+[Hb] = \frac{\mu_a^{\lambda_1}\varepsilon_{\Delta Hb}^{\lambda_2} - \mu_a^{\lambda_2}\varepsilon_{\Delta Hb}^{\lambda_1}}{\varepsilon_{Hb}^{\lambda_1}\varepsilon_{HbO_2}^{\lambda_2} - \varepsilon_{Hb}^{\lambda_2}\varepsilon_{HbO_2}^{\lambda_1}}, \quad (4)$$

where μ_a is the absorption coefficient; λ_1 and λ_2 are the two wavelengths; ε_{Hb} and ε_{HbO_2} are the known molar extinction coefficients of the oxy- and deoxy-hemoglobin, respectively; and $[Hb]$ and $[HbO_2]$ are, respectively, the concentrations of the two forms of hemoglobin.

The functional images of SO_2 and HbT corresponding to the two statuses are shown in Figs. 1(C)-(F). When the status of the rat was altered from the hyperoxia to the hypoxia, the SO_2 in the cerebral cortical venous vessels decreased. The average SO_2 levels were ~86% and ~61% under the hyperoxia status and the hypoxia status, respectively. Simultaneously, the HbT in the cerebral cortical venous vessels increased as a result of this alternation. The average HbT value under the hypoxia status was about ~11% greater than that under the hyperoxia status.

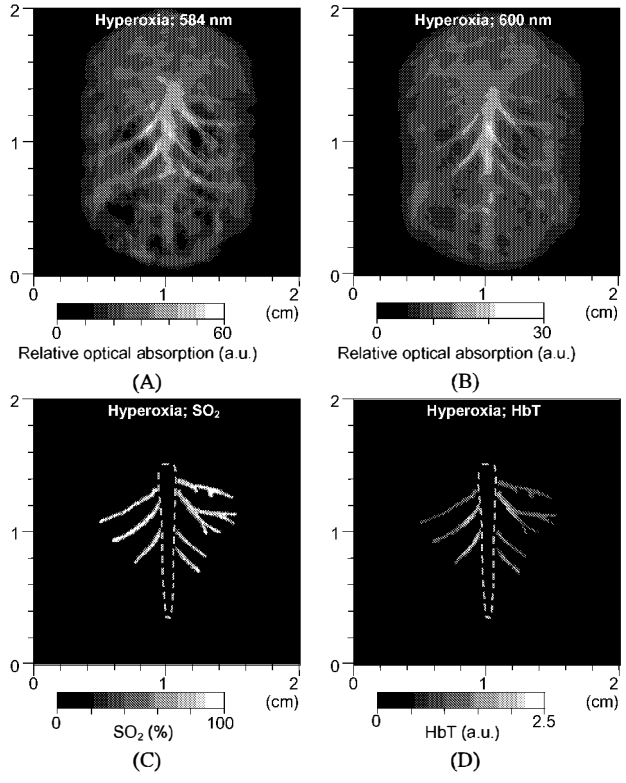

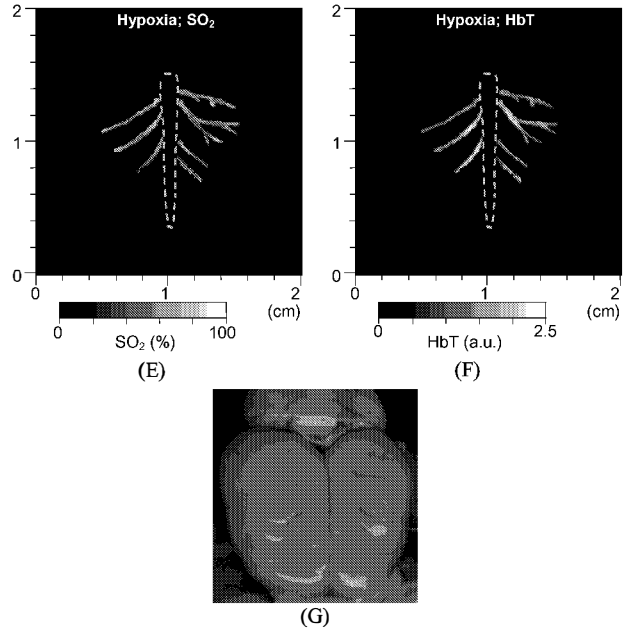

Fig. 1 (A) and (B), Images of the cerebral cortex of a rat brain generated by the 584-nm and 600-nm laser light respectively under the hyperoxia status. (C) and (D), Images of SO_2 and HbT in the cortical venous vessels under the hyperoxia status. (E) and (F), Images of SO_2 and HbT under the hypoxia status. (G), Open-skull anatomical photograph of the rat brain.

IV. SUMMARY

We developed rigorous reconstruction algorithms, the foundation for PAT. We accomplished non-invasive transdermal and transcranial imaging of small-animal brains *in vivo* showing both structures and functions. Based on the spectroscopic differences between oxy- and deoxy-hemoglobins, PAT can enable accurate functional imaging of cerebral blood oxygenation and blood volume in small-animal brains with satisfactory spatial resolution.

V. ACKNOWLEDGEMENTS

This project was sponsored in part by the U.S. Army Medical Research and Materiel Command Grant No. DAMD17-00-1-0455, the National Institutes of Health Grants No. R01 EB000712 and No. R01 NS46214, and Texas Higher Education Coordinating Board Grant No. ARP 000512-0063-2001.

VI. REFERENCES

1. M. Xu and L.-H. Wang, "Time-domain reconstruction for thermoacoustic tomography in a spherical geometry," IEEE T. Med. Imag. **21**, 814–822 (2002).
2. Y. Xu, D. Feng, and L.-H. Wang, "Exact frequency-domain reconstruction for thermoacoustic tomography—I: Planar geometry," IEEE T. Med. Imag. **21**, 823–828 (2002).
3. Y. Xu, M. Xu, and L.-H. Wang, "Exact frequency-domain reconstruction for thermoacoustic tomography—II: Cylindrical geometry," IEEE T. Med. Imag. **21**, 829–833 (2002).
4. X. Wang, Y. Pang, G. Ku, X. Xie, G. Stoica, and L.-H. Wang, "Non-invasive laser-induced photoacoustic tomography for structural and functional imaging of the brain *in vivo*," Nat. Biotech. **21**, 803–806 (2003).